Acta Biomaterialia 10 (2014) 2792–2803

Contents lists available at ScienceDirect

Acta Biomaterialia

journal homepage: www.elsevier.com/locate/actabiomat

Odontogenic differentiation and dentin formation of dental pulp cells under nanobioactive glass induction

Sainan Wang [a], Xuejun Gao [a], Weiyu Gong [a], Zhichun Zhang [a], Xiaofeng Chen [b], Yanmei Dong [a,*]

[a] Department of Cariology and Endodontology, Peking University School and Hospital of Stomatology, 22 Zhongguancun Nandajie, Haidian District, Beijing 100081, People's Republic of China

[b] National Engineering Research Center for Tissue Restoration and Reconstruction, South China University of Technology, Guangzhou 510640, People's Republic of China

ARTICLE INFO

Article history:
Received 14 October 2013
Received in revised form 20 December 2013
Accepted 5 February 2014
Available online 25 February 2014

Keywords:
Bioactive glass
Dental pulp cells
Odontogenic differentiation
Dentin regeneration
Nanoparticles

ABSTRACT

Bioactive glass (BG) has been widely used in bone regeneration; however, reports on the biological effects of BG on dental pulp cells are rare. This study aims to investigate the effects of nanoscale BG (n-BG) on odontogenic differentiation and dentin formation of dental pulp cells and to compare these effects with those of microscale BG (m-BG). Human dental pulp cells (hDPCs) from third molars were cultured directly with m-BG and n-BG in vitro. The cell proliferation increased at 0.1 mg ml^{-1} BG, which also had a chemotactic effect on hDPCs. The mineralization capacity and expression of odontogenic-related proteins and genes (dentin sialophosphoprotein, dentin matrix protein 1 and collagen type I) of hDPCs were significantly up-regulated under BG induction, and were particularly higher in the n-BG group than in the control group. m-BG and n-BG combined with pulp tissues were transplanted into the dorsum of immunodeficient mice to observe their biological effects on dental pulp cells in vivo. A continuous layer of dentin-like tissue with uniform thickness, a well-organized dentinal tubule structure and polarizing odontoblast-like cells aligned along it was generated upon the n-BG layer, whereas some irregular sporadic osteodentin-like mineralized tissues were observed in the control group. This study reveals that BG, especially n-BG, induces the odontogenic differentiation and dentin formation of dental pulp cells and may serve as a potential material for pulp repair and dentin regeneration.

1. Introduction

As a third-generation biomaterial, bioactive glass (BG) has osteoconductive and osteoinductive properties. BG can induce osteoblast differentiation, thereby making this material suitable for bone tissue repair and engineering applications [1–5]. A hydroxycarbonate apatite (HCA) layer is formed on the surface of BG following the initial dissolution of the material when exposed to biological fluid. This HCA layer is thought to interact with cells and collagen fibrils, and is responsible for the strong bond between the BG and the host tissue [6]. Ionic dissolution products from BG (e.g. Si, Ca, P) are directly linked to its function. Seven families of genes were up-regulated and activated within 48 h when osteoblasts were exposed to the ionic dissolution products of BG, including osteogenic-related transcription, cell cycle regulators, extracellular matrix components and growth factors [7,8].

As mineralized tissues, bone and dentin both have hydroxyapatite crystals and collagen as their main matrices. BG can reportedly enhance the expression of several mineralization-related genes (e.g. osteocalcin, osteonectin, osteopontin and bone sialoprotein) and promote alkaline phosphatase (ALP) activity and collagen type I (Col I) formation [9–11]. These proteins also make functions in dentin formation. Given the similarity of bone and tooth formation, BG could have an effect on dentin regeneration. In our previous research, we confirmed that the ionic dissolution of BG has good biocompatibility and increases the ALP expression of human dental pulp cells (hDPCs) [12]. In the present work, we further investigate the effect of BG on odontogenic differentiation in vitro and dentin formation in vivo.

Stem cells and progenitor cells are sensitive to their microenvironment and are capable of acquiring signals from nanotopography [13,14]. Mesenchymal cells and osteogenic precursor cells reportedly change their morphology when adhered to nanotopographical materials, and the expression levels of osteocalcin and osteopontin also increase [15,16]. Since the extracellular matrix and mineral crystals in dental tissue have nanoscale patterning, nanotechnology could be useful in improving the properties of materials. Nanoparticles have been used in a number of dental applications. As well as being used to improve their mechanical

* Corresponding author. Tel.: +86 10 82195475; fax: +86 10 62173402.
E-mail address: kqdongyanmei@bjmu.edu.cn (Y. Dong).

http://dx.doi.org/10.1016/j.actbio.2014.02.013
1742-7061/

properties of dental restoration materials, nanoparticles have also been investigated as carriers for drug, protein and gene delivery [17–20]. Nano-CaF_2 has been used as an effective anticaries agent, leading to a greater amount of F being incorporated in the apatitic formation compared with the macro-CaF_2 [21]. Biomimetic nanohydroxyapatite also possesses similar characteristics to the natural building blocks of tooth, so that it may be used as a repair material for dentin or enamel remineralization [22,23]. Nanoparticles have also been coated on dental implants to enhance their bioactive fixation to alveolar bone [24,25]. Sol–gel BG prepared with nanoscale topography has large surface areas and pore volumes, which result in the quick release of ions and high apatite nucleation rates. These characteristics endow the material with high bioactivity [26]. With the same composition, nanoscale BG (n-BG) has better biocompatibility and stronger osteogenesis ability than microscale BG (m-BG) [27,28].

Inducing odontogenic differentiation and dentin formation is extremely important in pulp repair and tooth regeneration. The objective of the present study is to investigate the effects of a novel n-BG on odontogenic differentiation and dentin formation of dental pulp cells. The resulting effects are then compared with those of m-BG. The proliferation, apoptosis, chemotaxis, mineralization and differentiation ability of hDPCs cultured with m-BG and n-BG are systematically tested in vitro. The effects of dentin formation under m-BG and n-BG induction are evaluated in vivo.

2. Materials and methods

2.1. Preparation and characterization of m-BG and n-BG

2.1.1. Preparation of m-BG and n-BG

The m-BG and n-BG sol–gel particles (molar composition: 58% SiO_2, 33% CaO, 9% P_2O_5) were prepared according to the procedure reported in previous works [26,29]. The preparation processes of m-BG and n-BG are shown in Fig. 1. Briefly, a sol was produced by the hydrolysis of tetraethyl orthosilicate (TEOS), triethylphosphate and calcium nitrate tetrahydrate (CN). After aging the sol at 70 °C for 3 days, followed by drying at 150 °C for 2 days, a gel was obtained. The gel was then heated for 2 h at 700 °C and became the sol–gel 58S m-BG. The synthesis procedure for the n-BG is as follows. TEOS (221.02 ml) and CN (138.68 g) were mixed with ethanol absolute (EA) (162.21 ml, ethanol:deionized water = 1:1) to form a solution; hydrochloric acid was used to adjust the pH between 1 and 2. A diammonium phosphate (DAP) solution containing 17.4 g of DAP in deionized water (162 ml) was also prepared. The TEOS–CN–EA solution was slowly added to the DAP solution whilst stirring. Once the two solutions were completely mixed, a solution of ammonia (28 wt.%, a gelation catalyst) was added dropwise to the mixture until a white precipitate appeared. Finally, the n-BG was obtained after freeze drying the sol–gel coprecipitate and heating at 600 °C.

2.1.2. Surface morphology and elemental composition of m-BG and n-BG by scanning electron microscopy and energy-dispersive X-ray spectroscopy

The m-BG and n-BG particles were coated with Au for 5 min under a gas pressure of 50 mtorr. The surface morphology of the particles was then observed by field-emission scanning electron microscopy (FE-SEM; S4800, JEOL, Japan). The surface elemental composition of the BG was evaluated using an energy-dispersive X-ray spectroscopy (EDX) detector attached to the FE-SEM instrument. Three independent regions were tested for each group.

2.1.3. Surface area and pore structure of m-BG and n-BG by N_2 adsorption experiments

The measurements of surface area and pore structure were carried out by N_2 adsorption experiments at 77.3 K on a Nova adsorption apparatus (Nova 4200e, Quantachrome, USA). The specific surface area of the particles was calculated from the Brunauer–Emmett–Teller plot of the adsorption–desorption isotherm using adsorption points in the P/P_0 range from 0.06 to 0.4 (NOVAWin software). Pore volumes were obtained from the volumes of N_2 adsorbed at $P/P_0 = 0.94$ or thereabouts. The average pore diameter was determined by the fourfold related total pore volume divided by the related surface area. Tests were conducted three times.

2.2. The biological effects of m-BG and n-BG on hDPCs in vitro

2.2.1. m-BG and n-BG coating

After high-temperature sterilization, the m-BG and n-BG powders were prepared as slurries of 0.01%, 0.05%, 0.1%, 0.5%, 1% and 5% (w/v) in deionized and distilled water. Exactly 100 and 2972 μl of slurry were respectively added to wells of a 96- and a 6-well polystyrene tissue culture plate (Costar, USA) to produce an equal surface coating of BG (Table 1). The plates were air dried in a laminar airflow cabinet to produce a stable adherent layer of m-BG and n-BG particles.

2.2.2. hDPCs culture

The hDPCs were derived from impacted fully developed healthy human third molars, which were collected from 19- to 25-year-old patients at the Oral Surgery Department of Peking University School and Hospital of Stomatology after informed consent and ethics permission (Reference No. PKUSSIRB-2013014) had been obtained. The extracted pulp tissues were minced and digested in a solution containing 3 mg ml^{-1} collagenase type I (Sigma, St. Louis, MO) and 4 mg ml^{-1} dispase (Sigma) for 30 min at 37 °C. The hDPCs were then transferred to sterile regular medium (Dulbecco's modified Eagle's medium, DMEM; Gibco, Gaithersburg, MD, USA), supplemented with 10% fetal bovine serum (Hyclone, USA), 100 U ml^{-1} penicillin and 100 μg ml^{-1} streptomycin at 37 °C in 5% CO_2. Cells were subcultured at a ratio of 1:3 upon reaching 75–85% confluence. The hDPCs at passages 3–5 were seeded on plates with or without the BG coating for further experiments (Fig. 2A).The medium was changed every 2 days. Cells were routinely examined under a phase-contrast inverted microscope (Olympus, Tokyo, Japan).

2.2.3. Cell chemotaxis of hDPCs by transwell chemotaxis assay

Transwell chambers with 8 μm pore polycarbonate membranes (Corning, New York, NY, USA) were used to evaluate cell chemotaxis. The hDPCs (5×10^4) were seeded into the upper compartment of the chambers. In the lower compartment, 0.1 mg ml^{-1} of m-BG and n-BG was coated on the bottom. Cells were allowed to migrate for 24 h to allow for the initial degradation of BG. The cells migrating to the lower side of the filter were fixed with 4% paraformaldehyde for 30 min, stained with crystal violet for 20 min and counted under a microscope in seven predetermined fields. All experiments were independently repeated three times.

2.2.4. Cell growth curve of hDPCs by MTT assay

hDPCs (5×10^3) were seeded in the wells of 96-well plates coated with different concentrations of m-BG or n-BG. A plate without BG coating served as the control. After 1, 3, 5, 7, 9 and 11 days of culture, an MTT (3-(4,5-dimethylthiazol-2-yl)-2,5-diphenyl-2,5-tetrazolium bromide) assay was carried out to investigate the metabolic activity of cells. The optical density (OD) was then measured at 570 nm using a microtiter plate reader (Titertek, Helsinki, Finland). Three independent experiments were

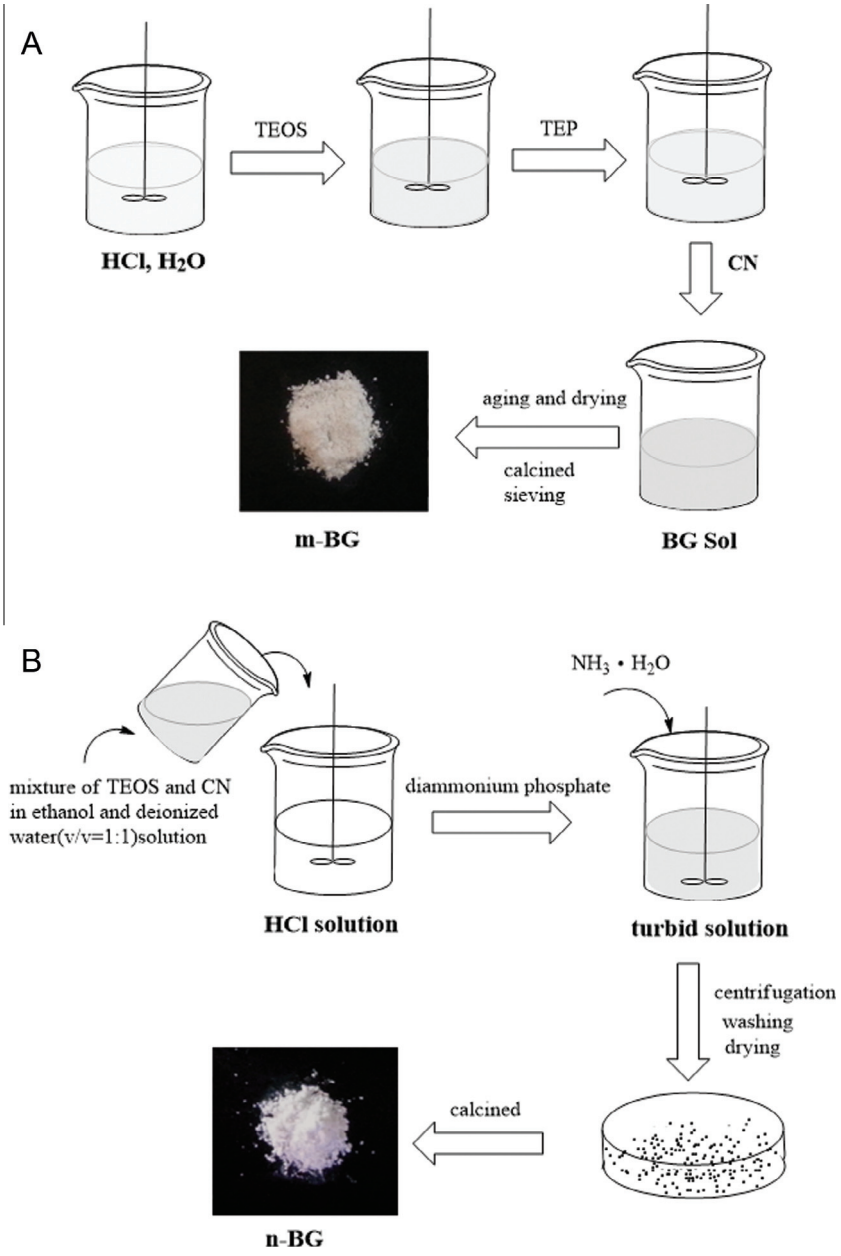

Fig. 1. Schematic diagram of the preparation process of m-BG (A) and n-BG (B). Abbreviations: CN, calcium nitrate tetrahydrate; TEOS, tetraethyl orthosilicate; TEP, triethylphosphate.

Table 1
Quantities of m-BG and n-BG coated on tissue culture plates.

% (w/v)	5%	1%	0.05%	0.01%	0.5%	0.1%
mg cm^{-2}	15.625	3.125	1.5625	0.3125	0.15625	0.03125

performed for each group. The graph was plotted using average values.

2.2.5. Cell cycle of hDPCs by flow cytometry

hDPCs (1×10^6) cultured with and without 0.1 mg ml^{-1} m-BG and n-BG were collected after 3 days. Cell precipitates were washed twice with 0.01 mol l^{-1} phosphate-buffered saline (PBS), resuspended in 1 ml of physiological saline, fixed in 2 ml of cold dehydrated alcohol and then stored at 4 °C overnight. Each sample was again washed with PBS and incubated with propidium iodide (100 mg ml^{-1}; Sigma) on ice for at least 30 min. Cell cycle fractions (G_0G_1, S and G_2M phases) were determined by flow cytometry (FCM). Three independent experiments from different donors were performed for each group.

2.2.6. Cell apoptosis of hDPCs by terminal deoxynucleotidyl transferase-mediated deoxyuridine triphosphate nick-end labelling assay

The hDPCs cultured with and without 0.1 mg ml^{-1} m-BG and n-BG were fixed with 4% paraformaldehyde in PBS for 1 h at room temperature. The apoptotic cell death was assessed by terminal deoxynucleotidyl transferase-mediated deoxyuridine triphosphate nick-end labelling (TUNEL) assay according to the manufacturer's protocol (Roche Boehringer–Mannheim, IN, USA). Then cells were counterstained with DPP (1:200, Santa Cruz) and Hoechst 33342 (Sigma). Hydrogen peroxide (H_2O_2) irritation was employed as

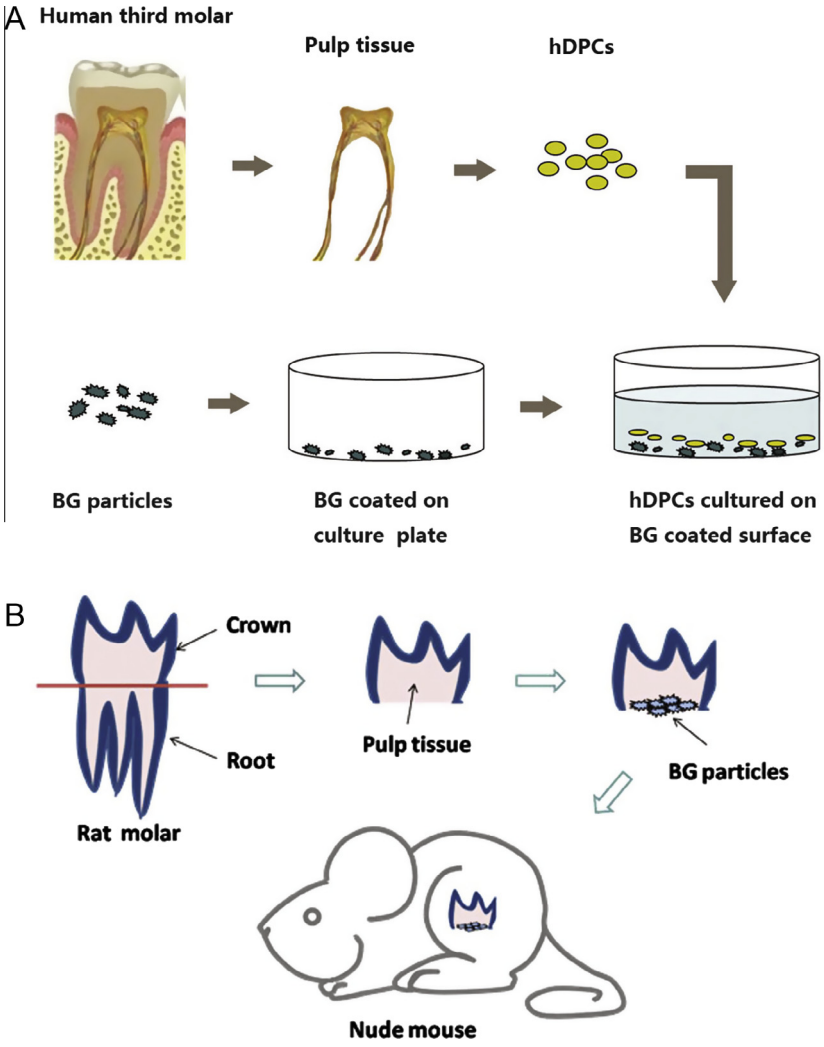

Fig. 2. Schematic diagram of in vitro and in vivo experiments. (A) Schematic diagram of hDPCs cultured with m-BG and n-BG in vitro; (B) model of subcutaneous transplantation in nude mouse in vivo.

positive control. Immunofluorescence staining was visualized under an Olympus FV1000 confocal laser scanning microscope (Olympus).

2.2.7. Mineralization ability of hDPCs by alizarin red staining

BG extract was acquired by soaking 0.1 mg ml^{-1} m-BG and n-BG in DMEM osteogenic-induced medium containing 10 mmol l^{-1} β-glycerophosphate (Sigma–Aldrich), 0.2 mmol l^{-1} ascorbate-2-phosphated (Sigma–Aldrich) and 100 nmol l^{-1} dexamethasone (Sigma–Aldrich) for 24 h. Sterile filtration was then employed to remove the particles. The BG extract was used to culture hDPCs for 4 weeks. Alizarin red staining was then carried out, and images were observed under a microscope. Alizarin red was destained with 10% cetylpyridinium chloride in 10 mmol l^{-1} sodium phosphate for 30 min at room temperature. The calcium concentrations were determined according to absorbance at 562 nm using a standard calcium curve prepared in the same solution. The final calcium levels in each group were normalized with the total protein concentrations obtained from the duplicate plates.

2.2.8. Odontogenic-related gene expression of hDPCs by real-time reverse transcription–polymerase chain reaction

The total cellular RNA of the three groups was obtained by adding TRIzol reagent (Invitrogen, Carlsbad, CA, USA) to the cell samples and then reverse transcribed using the SuperScript® III cDNA Synthesis Kit (Invitrogen). Real-time reverse transcription–polymerase chain reaction (RT-PCR) was performed using a SYBR® Premix Ex Taq™ Kit (TaKaRa, Bio, Otsu, Japan) and the ABI 7700 real-time PCR system. The primer sets used to detect dentin sialophosphoprotein (DSPP), dentin matrix protein 1 (DMP-1) and glyceraldehyde-3-phosphate dehydrogenase (GAPDH) are listed in Table 2. The real-time RT-PCR conditions were as follows: 95 °C for 10 min, followed by 40 cycles at 95 °C for 15 s and 60 °C for

Table 2
Forward and reverse primers for reverse transcription-polymerase chain reaction.

Gene	GenBank No.	Sequences (5′–3′)	Size (bp)
DMP-1	NM_004407.3	Forward: AGGAAGTCTCGCATCTCAGAG Reverse: TGGAGTTGCTGTTTTCTGTAGAG	100
DSPP	NM_014208.3	Forward: ATATTGAGGGCTGGAATGGGGA Reverse: TTTGTGGCTCCAGCATTGTCA	136
GAPDH	NM_002046.3	Forward: GAAGGTGAAGGTCGGAGTC Reverse: GAGATGGTGATGGGATTTC	225

1 min. The results were calculated from three independent experiments.

2.2.9. Odontogenic-related protein expression of hDPCs by western blot analysis

After 7 or 14 days of culture, the culture plates with hDPCs and extracellular matrices on the bottom were washed twice with cold PBS and lysed in RIPA lysis buffer (Beyotime, China) containing 1 mmol l^{-1} phenylmethylsulfonyl fluoride. Protein concentrations were determined using a Bio-Rad protein assay kit (Pierce, Rockford, IL, USA). Exactly 30 μg of proteins per lane was loaded onto 8% SDS–PAGE gel for electrophoresis and then transferred onto PVDF membranes. Membranes were blocked at room temperature for 2 h with a blocking solution (5% w/v skim milk, 0.01 mol l^{-1} PBS, 0.1% Tween-20) and subsequently incubated overnight at 4 °C with primary polyclonal antibodies against Col I (1:400; Abcam, Cambridge, MA, USA), monoclonal antibody against DPP (1:400; Santa Cruz) and GAPDH (1:1000; Zhongshan, Beijing, China), followed by 1 h incubation with appropriate horseradish peroxidase conjugated secondary antibodies at 1:5000 (Santa Cruz). The membranes were then visualized by SuperSignal West Pico Chemiluminescent Substrate (Thermo, Rockford, IL, USA) and exposed by the ChemiDoc XRS System. GAPDH served as an internal control in these experiments.

2.3. The biological effects of m-BG and n-BG on dental pulp cells in vivo

All animal experiments were conducted according to the accepted standards of humane animal care and approved by the Animal Care Committee of Peking University (Reference No. LA2011–057). The crowns of molars from 4-week-old Sprague–Dawley rats, including hard tissue and coronal pulp, were obtained after the roots were removed from the tooth cervix. The margin of dentin was slightly higher than that of the pulp tissue to benefit the placement of BG. Disinfected m-BG and n-BG powders were placed on the cross-section of the coronal pulp as experimental samples. Crowns alone were used as controls. The experimental and control samples were implanted into the dorsum of immune-deficient mice to observe their biological effects on pulp cells in vivo (Fig. 2B). After 2 and 6 weeks of transplantation, the samples were retrieved, fixed in 4% polyoxymethylene, decalcified and then processed for Masson's trichrome (Baso Diagnostic Inc, Zhuhai, Guangdong, China) staining according to the manufacturer's recommended protocol.

2.4. Statistics

Quantitative results were expressed as mean ± SD. An independent sample *t*-test was performed with SPSS Windows v. 12.0 software. *p*-values less than 0.05 were considered statistically significant.

3. Results

3.1. Characterization of m-BG and n-BG

The surface morphology and microstructure of m-BG and n-BG particles examined by FE-SEM are shown in Fig. 3A and B. The m-BG particles presented irregular structures, with sizes ranging between 2 and 20 μm. By contrast, the n-BG particles were of regular spherical shape, with sizes of approximately 20 nm.

The EDX spectra (Fig. 3C and D) show that the surfaces of the m-BG and n-BG are composed of large amounts of silicon, some calcium and phosphate.

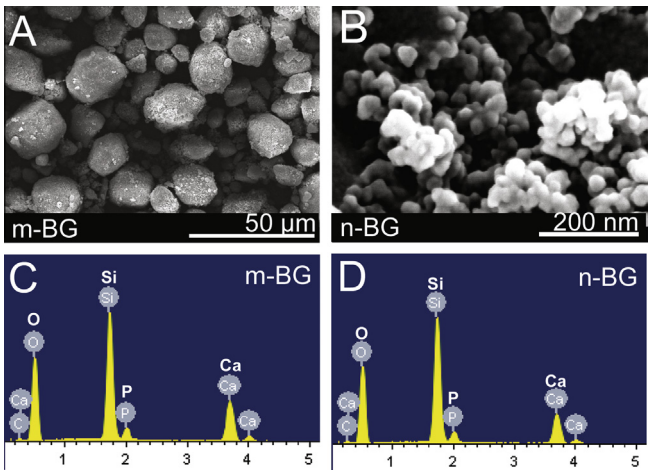

Fig. 3. Surface morphology and elemental composition of m-BG and n-BG Surface morphology of m-BG (A) and n-BG (B) by scanning electron microscopic analysis; surface elemental composition of m-BG (C) and n-BG (D) by energy-dispersive X-ray spectroscopy.

The surface areas, total pore volumes and average mesopore sizes of the two BG ascertained by N_2 adsorption experiments are shown in Table 3. The n-BG had an average mesopore size similar to that of m-BG, but had a larger surface area and a total pore volume that was twice that of m-BG.

3.2. The biological effects of m-BG and n-BG on hDPCs in vitro

3.2.1. Effects of m-BG and n-BG on the growth of hDPCs

Fig. 4B and C show the surfaces coated with 0.1 mg ml^{-1} m-BG and n-BG, respectively. The m-BG and n-BG particles aggregated into small clusters and were evenly distributed when coated on the bottom of the culture plates. Fig. 4E and F show that hDPCs grow around BG clusters, especially the n-BG clusters at the centre. The cells were uniformly distributed when BG was not coated on the bottom of the culture plates (Fig. 4D). The hDPCs maintained their characteristic morphology after incubation with BG compared with the control group.

hDPCs migrated through the polycarbonate membrane under m-BG and n-BG attraction, as shown in Fig. 4G–I. The statistical results from the three independent experiments show that the number of migrated cells was higher in both the m-BG and n-BG groups than in the control group (Figs. 5J).

3.2.2. Effects of m-BG and n-BG on the proliferation of hDPCs

The effects of different concentrations of BG on the proliferation of hDPCs were detected by MTT assay. The proliferation ability of hDPCs was enhanced by 0.1 mg ml^{-1} and lower concentrations of m-BG and n-BG compared with the control group. Significant inhibition of cell proliferation occurred in m-BG and n-BG at concentrations higher than 0.5 mg ml^{-1} ($p < 0.01$). The inhibitory effects gradually disappeared over time (Fig. 5A and B; the data for concentrations other than 0.1 and 0.5 mg ml^{-1} are not shown). The comparison of the OD values of different groups on days 5 and 7 (Fig. 5C) indicated that the inhibitory effect of n-BG was weaker than that of m-BG at 0.5 mg ml^{-1}. Therefore, 0.1 mg ml^{-1} BG was chosen for the subsequent experiments.

Table 3
The surface areas, total pore volumes and average pore diameters of m-BG and n-BG.

Sample	Surface area (m^2 g^{-1})	Total pore volume (cc g^{-1})	Average pore diameter (nm)
m-BG	28.020 ± 0.1	0.113 ± 0.01	15.5042 ± 0.02
n-BG	63.545 ± 0.2	0.230 ± 0.01	15.0104 ± 0.03

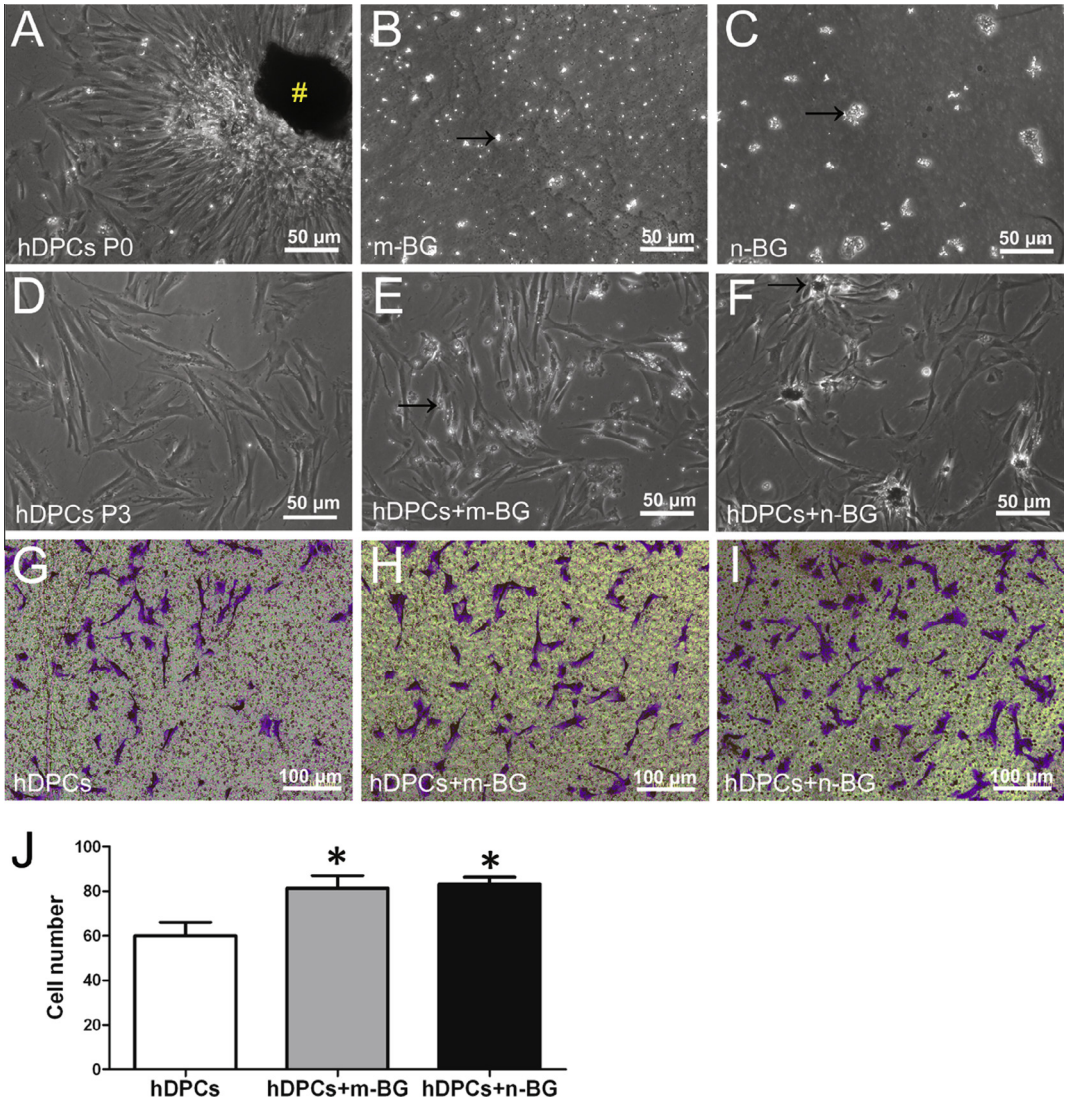

Fig. 4. Effects of m-BG and n-BG on the growth and chemotaxis of hDPCs (A) Primary hDPCs from human third molars; # indicates the block of original pulp tissue; tissue culture plate coated with (B) 0.1 mg ml^{-1} m-BG and (C) 0.1 mg ml^{-1} n-BG; (D) hDPCs at the third passage; hDPCs at the third passage cultured with (E) 0.1 mg ml^{-1} m-BG and (F) 0.1 mg ml^{-1} n-BG (black arrow indicates BG cluster); hDPCs migrating through the polycarbonate membrane of the transwell chamber in the (G) control group, (H) m-BG group and (I) n-BG group by crystal violet staining; (J) statistical analysis of the cell number in different groups by transwell chemotaxis assay. *indicates significant difference in the comparison between the m-BG or n-BG group and the control group ($p < 0.05$).

FCM was performed to further investigate the proliferation index, i.e. the percentage of cells in the S and G_2M phases. Fig. 5D–F show that the proliferation indices of hDPCs cultured with m-BG (S + G_2M = 18.37%) and n-BG (S + G_2M = 19.83%) on day 3 were significantly higher than in the control group (S + G_2M = 10.48%), thus indicating that 0.1 mg ml^{-1} BG promotes the proliferation of hDPCs.

3.2.3. Effects of m-BG and n-BG on the apoptosis of hDPCs

TUNEL staining was carried out to test whether BG induces the apoptosis of hDPCs (Fig. 6A–P). TUNEL-positive apoptotic cells (red fluorescence) showed in H_2O_2-irritated hDPCs but not in the m-BG, n-BG and control groups. Little DPP was expressed in the cytoplasm (green fluorescence) in the control group (Figs. 6C), whereas DPP could be detected in cells in both the m-BG and n-BG groups (Fig. 6G and K).

3.2.4. Effects of m-BG and n-BG on the mineralization and odontogenic differentiation of hDPCs

Alizarin red staining revealed the mineralized nodules generated after 4 weeks of osteogenic-inducing culture (Fig. 7A). The relative calcium concentrations significantly increased in the m-BG and n-BG groups, and were particularly higher in the n-BG group compared with that in the control group (Fig. 7B).

A comparison of the results of the control group reveals a statistical increase in *DSPP* and *DMP-1* gene expression in hDPCs cultured with BG on days 7 and 14; the effects of n-BG were stronger than those of m-BG (Fig. 7C). Western blot indicates that the quantity of total and mature Col I significantly increased in the two BG groups (Fig. 7D), especially higher in n-BG group than in control group. The amount of expressed DPP increased under m-BG and n-BG induction, particularly in the n-BG group after 14 days. The expected molecular weight of DPP is approximately 100 kDa [30,31] or 140 kDa [32].

3.3. Effects of m-BG and n-BG on dental pulp cells in vivo

In the control group the crowns were implanted alone, the pulp tissue remained normal, with a few irregular mineralized tissues generated, at 2 weeks. The osteoblast-like cells were parallel to the surface of the newly generated matrix, whereas osteocytes-like

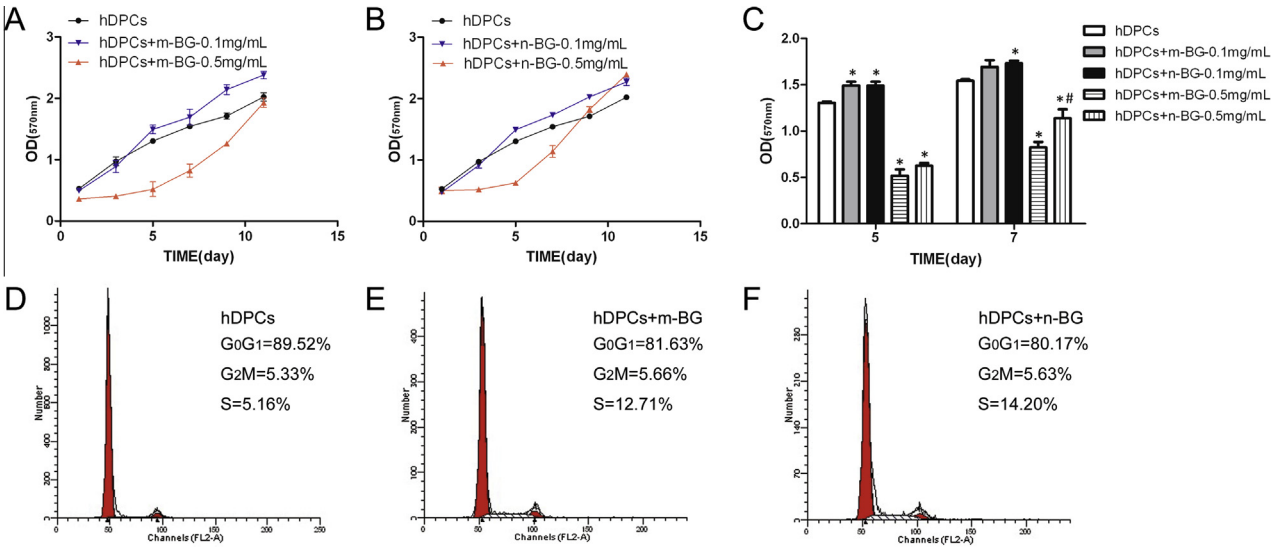

Fig. 5. Effects of m-BG and n-BG on the proliferation of hDPCs. Growth curves of hDPCs cultured with different concentrations of (A) m-BG and (B) n-BG as determined by MTT assay; (C) OD values of hDPCs cultured with m-BG and n-BG compared with untreated hDPCs from day 5 to day 7; representative cell-cycle distribution profiles of hDPCs cultured (D) without BG, (E) with 0.1 mg ml^{-1} m-BG and (F) with 0.1 mg ml^{-1} n-BG. *indicates significant difference in the comparison between the m-BG or n-BG group and the control group ($p < 0.05$); # indicates significant difference in the comparison between the m-BG group and the n-BG group ($p < 0.05$).

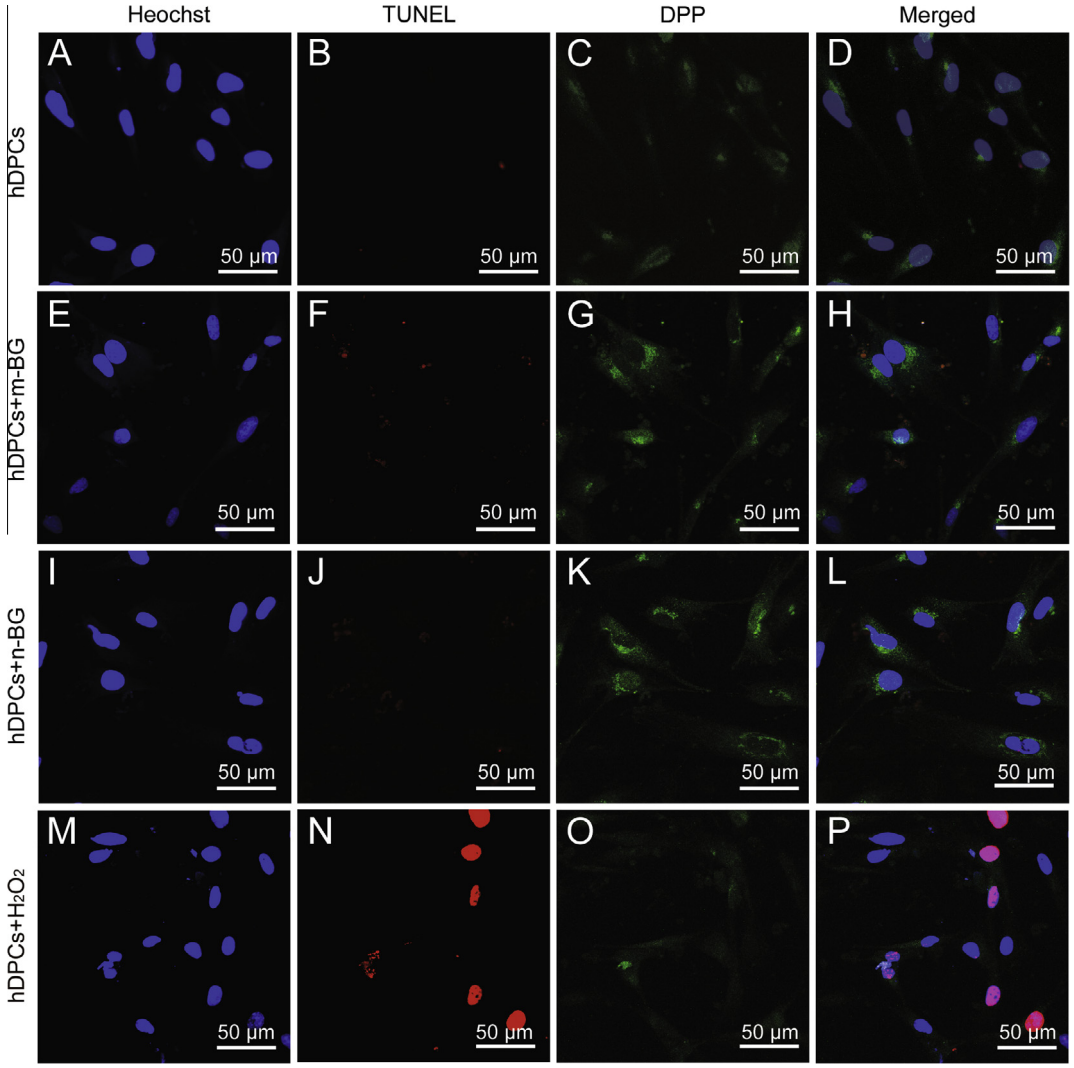

Fig. 6. Effects of m-BG and n-BG on the apoptosis of hDPCs. (A–D) TUNEL staining of hDPCs; (E–H) hDPCs cultured with 0.1 mg ml^{-1} m-BG; (I–L) hDPCs cultured with 0.1 mg ml^{-1} n-BG; (M–P) hDPCs irritated by H_2O_2. Nucleus: blue fluorescence; TUNEL-positive: red fluorescence in nucleus; DPP-positive: green fluorescence in cytoplasm.

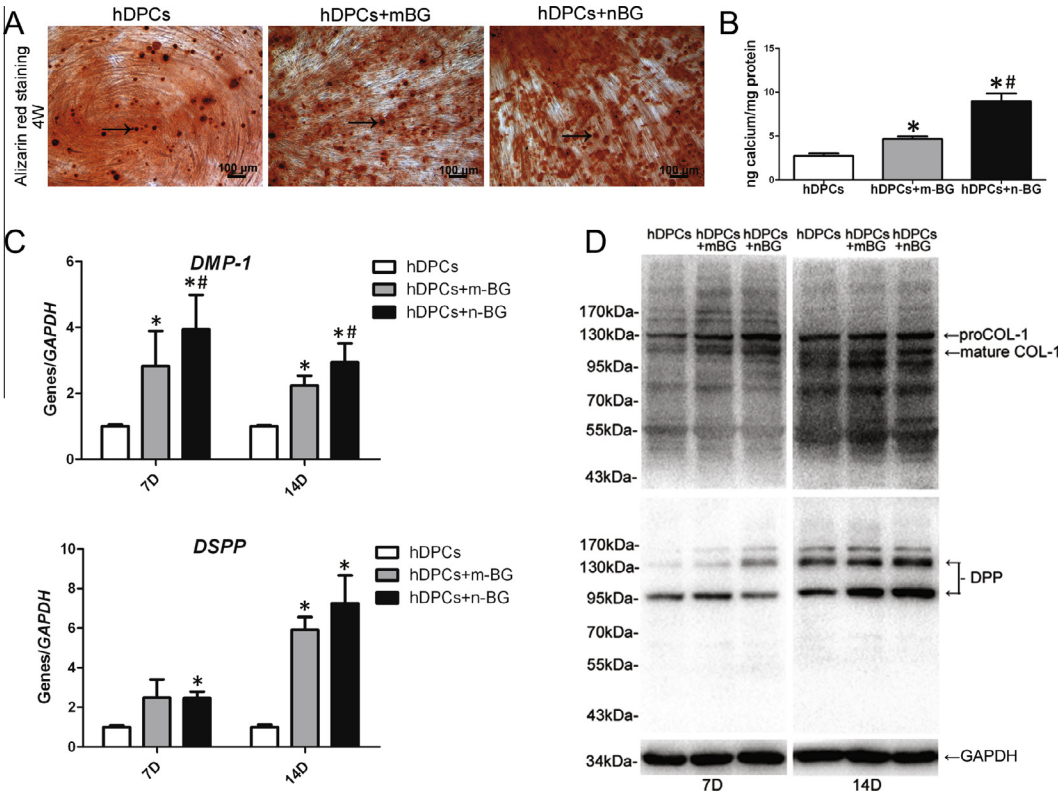

Fig. 7. Effects of m-BG and n-BG on the mineralization and odontogenic differentiation of hDPCs. (A) Alizarin red staining of mineralized nodule after 4 weeks of osteogenic-inducing culture in hDPCs cultured with and without BG. The red block mass marked by the black arrow shows the mineralized nodule; (B) calcium concentrations in different groups by cetylpyridinium chloride detection; (C) RT-PCR results of gene expression in hDPCs cultured with and without m-BG and n-BG for DSPP and DMP-1. GAPDH was used as an internal control. Gene expression was described as fold changes relative to the control group at the same time point. Values show the mean ± SD of $n = 3$; (D) Western blot results of Col I and DPP protein levels in hDPCs cultured with and without m-BG and n-BG. GAPDH was used as a loading control. * indicates significant difference in the comparison between the m-BG or n-BG group and the control group ($p < 0.05$); # indicates significant difference in the comparison between the m-BG group and the n-BG group ($p < 0.05$).

cells were observed among the mineralized tissues (Fig. 8A and B). More sporadic osteodentin-like mineralized deposits were observed after 6 weeks. Some irregular dentin formed below the primary dentin of the crown (Fig. 8C and D).

In the n-BG group, newly generated matrix was observed around n-BG particles and was integrated into a whole layer in the pulp material interface at 2 weeks. Polarizing odontoblast-like cells were found aligned along this layer, and their long axes were perpendicular to the surface of the new matrix. In addition, a new thin layer of dentin was detected below the primary dentin; this was not observed in the control group. The pulp tissue remained normal and comprised many blood vessels (Fig. 8E and F). After 6 weeks, thick and well-organized dentin-like matrix aligned with differentiated columnar odontoblast-like cells was observed upon the n-BG layer; this new dentin-like tissue was continuous with uniform thickness. Odontoblastic processes were embedded in the mineralized tissue, and reached the entire layer of the new matrix. A new layer of dentin was also seen below the crown primary dentin and integrated with the dentin-like tissue above the n-BG. Material degradation occurred at the n-BG cluster (Fig. 8G and H). Pulpo-dentinal complex-like tissue was also generated on the material layer in the m-BG group by 6 weeks. However, the new dentin-like tissue was thinner than that in n-BG group and did not completely surround the material layer (Fig. 8I and J).

4. Discussion

In this study, both n-BG and m-BG at low concentrations promoted pulp cells proliferation, and at higher concentrations slowed the cell proliferation, though the inhibitory effects diminished with time. However, the cell number in the n-BG group surpassed that in the control group at later time points. This may be caused by the formation of an HCA layer, which decreases the release of ions or changes the pH to facilitate cell growth. In an earlier study, Salako et al. [33] tested 45S5 BG as a pulpotomy agent in rat molars. They found that BG caused a phase of acute inflammation or even necrosis of pulp, following which there was a recovery period during which restoration of pulp morphology was possible. That was probably via a similar mechanism to the one found in our study with the higher concentration of BG. It has been reported that the release of an appropriate quantity of ions by BG promoted cell proliferation, while higher concentrations were toxic for cells growth [5,34]; for example, a higher Ca concentration (of 88–109 ppm) has been shown to reduce osteoblast proliferation [35].

Adhesion is an important step at the beginning of cell–material interaction, and is also a foundation for cell growth, proliferation and differentiation. In this study, hDPCs were chemotactically attracted towards and grew with the two types of BG. This was particularly so with the n-BG, where cells grew with n-BG clusters as the centre. This was demonstrated again by the in vivo experiment. In vivo, a row of polarizing odontoblast-like cells was formed along the n-BG surface as well as the m-BG surface when the pulp tissue (combined with BG) was subcutaneously implanted. The cells aligned more regularly on the n-BG surface than on the m-BG. This suggests that n-BG could be capable of attracting and inducing pulp stem cells/progenitor cells to adhere and organize in an orderly manner. This could be attributed to the ions (Si, Ca and so on) released by the BG. Some progenitor cells (e.g. bone marrow progenitor cells and endothelial progenitor cells) reportedly

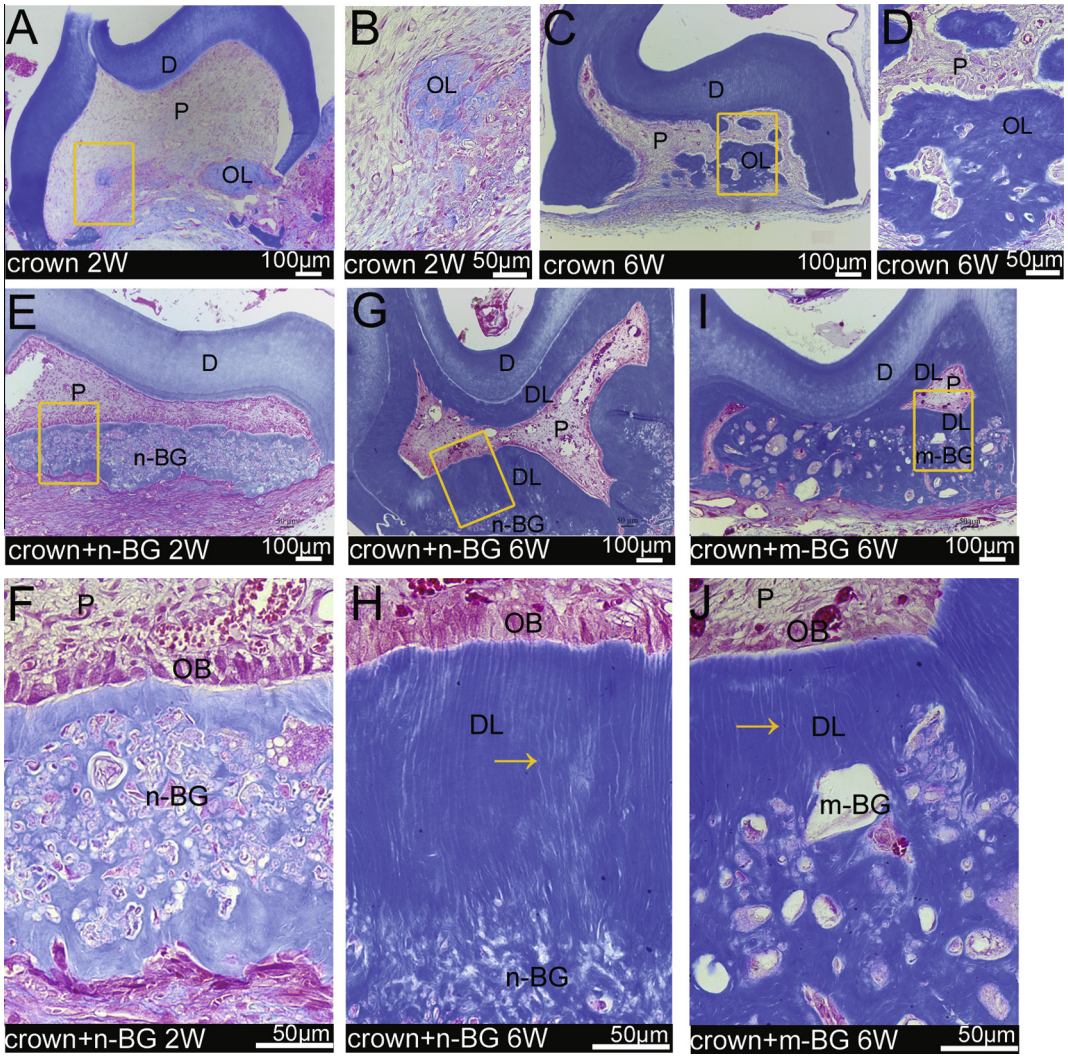

Fig. 8. Masson's trichrome staining evaluation of the effects of m-BG and n-BG on dentin formation. (A, B) (B is a magnified image of A) Crowns implanted alone for 2 weeks; (C, D) crowns implanted alone for 6 weeks; (E, F) crowns covered with n-BG after 2 weeks of transplantation; (G, H) crowns covered with n-BG after 6 weeks of transplantation; (I, J) crowns covered with m-BG after 6 weeks of transplantation. The yellow arrow points to the odontoblastic processes embedded in the newly generated dentin-like matrix. Abbreviations: D, dentin; DL, dentin-like tissues; m-BG, microbioactive glass; n-BG, nanobioactive glass; OB, odontoblast-like cells; OL, osteodentin-like tissues; P, pulp tissue.

mobilize to sites with high calcium concentration, possibly through a calcium-sensing receptor-mediated signal pathway [36,37]. The surface properties of the material, including charge, wettability and nanotopography, could also affect cell adhesion [38,39]. The nanostructure would probably enhance the surface characteristics and the release of ions compared with the microstructure.

Aside from inducing adhesions of dental pulp cells, n-BG further promoted the generation of odontoblast-like cells to form a continuous layer of dentin-like tissue with well-organized dentinal tubules. The m-BG also has this ability, but the generated dentin was thinner and less regular than in the n-BG group. This suggests that the bioglass materials could create a suitable microenvironment to support odontogenic differentiation and dentin formation, and the effects would be much stronger with n-BG. Unlike other hard tissues, the long odontoblast process embedded in the new mineralized matrix in this study helps the pulp tissue to rebuild its functional protection and sensation mechanisms (this typical pulpo-dentin complex tissue is a unique characteristic of tooth). Although bone and dentin have similar compositions, they have different origins; dental pulp cells originate from neural crest ectomesenchyme and experience epithelial–mesenchymal interactions during development, whereas osteoblasts of limb bone derive from somatic mesenchyme. A significant difference of the pulp-dentin complex in comparison with bone is that odontoblasts growing along the border of the mineralization front are polarized, with the cell bodies aligned towards, and the cell processes embedded in, the mineralized matrix. Unlike osteocytes, the cell body of an odontoblast is never entrapped in its matrix. Expressions of different non-collagenous proteins are believed to be responsible for initiating and modulating the mineralization of dentin and bone. The in vitro study demonstrated that n-BG, particularly compared with BG, could up-regulate the mineralization capacity and expression of DSPP and DMP-1 in hDPCs. DSPP, the major non-collagenous matrix protein in dentin, is involved in the nucleation and control of the hydroxyapatite mineral phase during dentin calcification [40,41]. DPP has also been detected in bone, but only at a level 1/400th of that of dentin. DPP has been considered as being implicated in tubular dentin mineralization and as a differentiation marker of odontoblast lineages [42–44]. DMP-1, a multifunctional protein originally extracted from rat odontoblasts [45], regulates the mineralization of dentin through the nucleation

of hydroxyapatite crystals [46] and has high binding affinity towards collagen fibrils [47]. This protein also takes part in the regulation of phosphate homeostasis [48] and the differentiation of odontoblasts [49–51]. The up-regulation of these markers in hDPCs, induced by n-BG and m-BG, would promote odontogenesis. The nanostructure of n-BG gives it a greater ability to induce odontogenic-related proteins, which led to the faster and thicker dentin formation seen in this study.

In summary, the novel n-BG used in our study shows better performance than m-BG with regard to dentin formation. n-BG clusters can attract pulp cells to grow around them in cell culture, and promote greater mineralization and expression of odontoblast-related markers than the m-BG. There is also evidence that thicker dentin was formed under the n-BG induction compared with the m-BG. Possible mechanisms for the better performance by the n-BG in dentinogenesis are as follows. The particle size of the n-BG used in the present study is about 20 nm, and the particles have a spherical shape; such a size is reportedly beneficial for cell proliferation and activity [52]. Aggregated BG nanoparticles could increase the number of binding sites available on the material surface, and could promote electrostatic interactions between the proteins and this surface, thereby enhancing protein adsorption [53]. Protein adsorption would influence cell adhesion by the adsorption of key adhesion molecules. The nanoscale n-BG surface could improve the initial cell attachment, facilitating the adhesion of collagen molecules and promoting the nucleation and growth of hydroxyapatite crystals [54,55]. The large specific surface area of n-BG could render these particles highly reactive, thus leading to the rapid release of ions and increasing the apatite nucleation rate [26,27,56].

From the in vivo results, odontoblast-like cells are seen to align on the surface of the n-BG layer more regularly. This could be attributed to the nanostructure, which would maintain the consistency of the odontoblast polarization and would regulate their arrangement. Further studies are required to explore the potential mechanism behind the regulatory ability of n-BG on hDPCs. Matching the degradation speed of the biomaterial with the generation of new tissue is an important factor in tissue regeneration. That n-BG particles degraded faster than m-BG could be attributed to their smaller particle size and higher dissolution ratio [56].

Inducing dentin formation is a clear strategy in endodontic treatment. Recently, mineral trioxide aggregate (MTA) has attracted increasing attention in the dental field. MTA has good sealing ability and biocompatibility, and it promotes the proliferation and mineralization of pulp cells [57]. The localized elevation of calcium ions released by MTA is suggested to be responsible for the increased expression of mineralization-promoting genes (osteopontin and bone morphogenic protein-2) in pulp cells [58]. Other synthesized inorganic materials, such as calcium phosphates, are also used to induce dentin formation [59–62]. In the present study, the newly generated dentin induced by the n-BG is continuous and complete, and has uniform thickness. Odontoblastic processes reached the entire layer of the new dentin. These results are different from the studies with MTA. As reported recently, the generated dentin induced by MTA or other materials often has irregular thickness and morphology. Although some odontoblast-like cells were discovered to be adjacent to the dentin bridge, with well-distinguishable dentin tubules, the tubules were often short or irregular [63–65]. The amorphous BG structure is generally more soluble and reactive than crystalline calcium phosphates, thereby accelerating the apatite formation process and enhancing the bioactivity of the material [66–68]. BG uniquely releases Si ions, which are essential to the formation and calcification of mineralized tissue [69,70]. Si ions stimulate osteogenic-related gene expression and extracellular matrix formation, which enhances osteoblastic differentiation [71–73]. BG is a biodegradable material that exhibits controlled breakdown and resorption. In this manner, the interface problems are solved because the foreign material is ultimately replaced by self-regenerating tissues. The uncertain effect caused by the long-term existence of exogenous material is also eliminated.

In the applications of BG in endodontics, previous investigators have histologically tested 45S5 BG for pulp capping, and demonstrated formations of reparative dentin bridge [74,75]. However, the reparative dentin bridges generated were atubular rather than tubular, as seen in normal dentin, due to superficial pulp-tissue necrosis caused by the capping agent. Whether the signals for the reparative action comes from the biomaterials or is just an intrinsic reaction to trauma is unclear. Compared with traditional melt-derived 45S5 BG, sol–gel-derived BG has the advantages of higher porosity, much larger surface areas and higher Si content, all of which enhance its bioactivity [76]. Compared with others bioglasses, the new generation sol–gel 58S BG used in this study, especially the nanoscale version, showed greater induction of pulp cell migration, surface attachment, proliferation and odontogenic differentiation, as demonstrated by a series of experiments combined with novel cytological, molecular biological and histological techniques.

5. Conclusions

Nanoscale BG induces dentin formation more strongly than microscale BG through the combined action of cell migration, surface attachment, polarization, odontogenic differentiation and mineralization of hDPCs, possibly due to the n-BG having a larger surface area, more binding sites, a faster dissolution rate, and many other chemical and biological properties. The n-BG may serve as a potential material for pulp repair and dentin regeneration.

Acknowledgements

The authors are grateful for the support of the National Natural Science Foundation of China (No. 51372005 and 81070800), the technical assistance of the Department of Biochemistry and Molecular Biology of Peking University School of Basic Medical Sciences and the helpful discussions with Prof. Chunyan Zhou, Drs. Zhuqing Jia and Weiping Wang.

Appendix A. Figures with essential colour discrimination

Certain figures in this article, particularly Figs. 1–8, are difficult to interpret in black and white. The full colour images can be found in the on-line version, at http://dx.doi.org/10.1016/j.actbio.2014.02.013.

References

[1] Hoppe A, Guldal NS, Boccaccini AR. A review of the biological response to ionic dissolution products from bioactive glasses and glass-ceramics. Biomaterials 2011;32:2757–74.
[2] Rahaman MN, Day DE, Bal BS, Fu Q, Jung SB, Bonewald LF, et al. Bioactive glass in tissue engineering. Acta Biomater 2011;7:2355–73.
[3] Bielby RC, Pryce RS, Hench LL, Polak JM. Enhanced derivation of osteogenic cells from murine embryonic stem cells after treatment with ionic dissolution products of 58S bioactive sol–gel glass. Tissue Eng 2005;11:479–88.
[4] Gough JE, Jones JR, Hench LL. Nodule formation and mineralisation of human primary osteoblasts cultured on a porous bioactive glass scaffold. Biomaterials 2004;25:2039–46.
[5] Valerio P, Pereira MM, Goes AM, Leite MF. The effect of ionic products from bioactive glass dissolution on osteoblast proliferation and collagen production. Biomaterials 2004;25:2941–8.
[6] Hench LL, Paschall HA. Direct chemical bond of bioactive glass-ceramic materials to bone and muscle. J Biomed Mater Res 1973;7:25–42.
[7] Christodoulou I, Buttery LD, Tai G, Hench LL, Polak JM. Characterization of human fetal osteoblasts by microarray analysis following stimulation with 58S bioactive gel-glass ionic dissolution products. J Biomed Mater Res B Appl Biomater 2006;77:431–46.

[8] Xynos ID, Edgar AJ, Buttery LD, Hench LL, Polak JM. Gene-expression profiling of human osteoblasts following treatment with the ionic products of Bioglass 45S5 dissolution. J Biomed Mater Res 2001;55:151–7.
[9] Varanasi VG, Owyoung JB, Saiz E, Marshall SJ, Marshall GW, Loomer PM. The ionic products of bioactive glass particle dissolution enhance periodontal ligament fibroblast osteocalcin expression and enhance early mineralized tissue development. J Biomed Mater Res, Part A 2011;98:177–84.
[10] Carvalho SM, Oliveira AA, Jardim CA, Melo CB, Gomes DA, de Fatima Leite M, et al. Characterization and induction of cementoblast cell proliferation by bioactive glass nanoparticles. J Tissue Eng Reg Med 2012;6:813–21.
[11] Tsigkou O, Jones JR, Polak JM, Stevens MM. Differentiation of fetal osteoblasts and formation of mineralized bone nodules by 45S5 Bioglass conditioned medium in the absence of osteogenic supplements. Biomaterials 2009;30:3542–50.
[12] Mi SS, Dong YM, Gao XJ. [Effects of ionic-dissolution of sol–gel bioactive glasses on human dental pulp cells] Beijing da xue xue bao Yi xue ban. J Peking Univ Health Sci 2012;44:39–42.
[13] McNamara LE, McMurray RJ, Biggs MJ, Kantawong F, Oreffo RO, Dalby MJ. Nanotopographical control of stem cell differentiation. J Tissue Eng 2010;2010:120623.
[14] Dalby MJ, Gadegaard N, Curtis AS, Oreffo RO. Nanotopographical control of human osteoprogenitor differentiation. Curr Stem Cell Res Ther 2007;2:129–38.
[15] Dalby MJ, McCloy D, Robertson M, Wilkinson CD, Oreffo RO. Osteoprogenitor response to defined topographies with nanoscale depths. Biomaterials 2006;27:1306–15.
[16] Biggs MJ, Richards RG, Gadegaard N, McMurray RJ, Affrossman S, Wilkinson CD, et al. Interactions with nanoscale topography: adhesion quantification and signal transduction in cells of osteogenic and multipotent lineage. J Biomed Mater Res, Part A 2009;91:195–208.
[17] Lee BS, Huang LC, Hong CY, Wang SG, Hsu WH, Yamauchi Y, et al. Synthesis of metal ion–histidine complex functionalized mesoporous silica nanocatalysts for enhanced light-free tooth bleaching. Acta Biomater 2011;7:2276–84.
[18] Saunders SA. Current practicality of nanotechnology in dentistry. Part 1. Focus on nanocomposite restoratives and biomimetics. Clin, Cosmetic Invest Dentist 2009;1:47–61.
[19] Kovtun A, Kozlova D, Ganesan K, Biewald C, Seipold N, Gaengler P, et al. Chlorhexidine-loaded calcium phosphate nanoparticles for dental maintenance treatment: combination of mineralising and antibacterial effects. RSC Adv 2012;2:870–5.
[20] Okada M, Furuzono T. Hydroxylapatite nanoparticles: fabrication methods and medical applications. Sci Technol Adv Mater 2012;13:064103.
[21] Sun L, Chow LC. Preparation and properties of nano-sized calcium fluoride for dental applications. Dent Mat: Offic Public Acad Dent Mat 2008;24:111–6.
[22] Tschoppe P, Zandim DL, Martus P, Kielbassa AM. Enamel and dentine remineralization by nano-hydroxyapatite toothpastes. J Dent 2011;39:430–7.
[23] Huang S, Gao S, Cheng L, Yu H. Remineralization potential of nano-hydroxyapatite on initial enamel lesions: an in vitro study. Caries Res 2011;45:460–8.
[24] Jimbo R, Coelho PG, Bryington M, Baldassarri M, Tovar N, Currie F, et al. Nano hydroxyapatite-coated implants improve bone nanomechanical properties. J Dent Res 2012;91:1172–7.
[25] Pang X, Huang Y. Physical properties of nano-HAs/ZrO_2 coating on surface of titanium materials used in dental-implants and its biological compatibility. J Nanosci Nanotechnol 2012;12:902–10.
[26] Lei B, Chen X, Wang Y, Zhao N, Du C, Fang L. Surface nanoscale patterning of bioactive glass to support cellular growth and differentiation. J Biomed Mater Res, Part A 2010;94:1091–9.
[27] de Oliveira AA, de Souza DA, Dias LL, de Carvalho SM, Mansur HS, de Magalhaes Pereira M. Synthesis, characterization and cytocompatibility of spherical bioactive glass nanoparticles for potential hard tissue engineering applications. Biomed Mater 2013;8:025011.
[28] Gong WY, Dong YM, Chen XF, Karabucak B. Nano-sized 58S bioactive glass enhances proliferation and osteogenic genes expression of osteoblast-like cells. Chin J Dent Res 2012;15:145–52.
[29] Lin C, Mao C, Zhang J, Li Y, Chen X. Healing effect of bioactive glass ointment on full-thickness skin wounds. Biomed Mater 2012;7:045017.
[30] Prasad M, Butler WT, Qin C. Dentin sialophosphoprotein in biomineralization. Connect Tissue Res 2010;51:404–17.
[31] Tsuchiya S, Simmer JP, Hu JC, Richardson AS, Yamakoshi F, Yamakoshi Y. Astacin proteases cleave dentin sialophosphoprotein (DSPP) to generate dentin phosphoprotein (DPP). J Bone Mineral Res: Offic J Am Soc Bone Mineral Res 2011;26:220–8.
[32] Chang SR, Chiego Jr D, Clarkson BH. Characterization and identification of a human dentin phosphophoryn. Calcif Tissue Int 1996;59:149–53.
[33] Salako N, Joseph B, Ritwik P, Salonen J, John P, Junaid TA. Comparison of bioactive glass, mineral trioxide aggregate, ferric sulfate, and formocresol as pulpotomy agents in rat molar. Dent Traumatol: Offic Publ Int Assoc Dent Traumatol 2003;19:314–20.
[34] Christodoulou I, Buttery LD, Saravanapavan P, Tai G, Hench LL, Polak JM. Dose- and time-dependent effect of bioactive gel-glass ionic-dissolution products on human fetal osteoblast-specific gene expression. J Biomed Mater Res B Appl Biomater 2005;74:529–37.
[35] Alcaide M, Portoles P, Lopez-Noriega A, Arcos D, Vallet-Regi M, Portoles MT. Interaction of an ordered mesoporous bioactive glass with osteoblasts, fibroblasts and lymphocytes, demonstrating its biocompatibility as a potential bone graft material. Acta Biomater 2010;6:892–9.
[36] Aguirre A, Gonzalez A, Navarro M, Castano O, Planell JA, Engel E. Control of microenvironmental cues with a smart biomaterial composite promotes endothelial progenitor cell angiogenesis. Eur Cells Mat 2012;24:90–106.
[37] Tommila M, Jokilammi A, Terho P, Wilson T, Penttinen R, Ekholm E. Hydroxyapatite coating of cellulose sponges attracts bone-marrow-derived stem cells in rat subcutaneous tissue. J Royal Soc, Interf/ Royal Soc 2009;6:873–80.
[38] Tsimbouri P, Gadegaard N, Burgess K, White K, Reynolds P, Herzyk P, et al. Nanotopographical effects on mesenchymal stem cell morphology and phenotype. J Cell Biochem 2013.
[39] Fiedler J, Ozdemir B, Bartholoma J, Plettl A, Brenner RE, Ziemann P. The effect of substrate surface nanotopography on the behavior of multipotnent mesenchymal stromal cells and osteoblasts. Biomaterials 2013;34:8851–9.
[40] McKnight DA, Simmer JP, Hart PS, Hart TC, Fisher LW. Overlapping DSPP mutations cause dentin dysplasia and dentinogenesis imperfecta. J Dent Res 2008;87:1108–11.
[41] Lee SK, Lee KE, Jeon D, Lee G, Lee H, Shin CU, et al. A novel mutation in the DSPP gene associated with dentinogenesis imperfecta type II. J Dent Res 2009;88:51–5.
[42] Sreenath T, Thyagarajan T, Hall B, Longenecker G, D'Souza R, Hong S, et al. Dentin sialophosphoprotein knockout mouse teeth display widened predentin zone and develop defective dentin mineralization similar to human dentinogenesis imperfecta type III. J Biol Chem 2003;278:24874–80.
[43] Suzuki S, Sreenath T, Haruyama N, Honeycutt C, Terse A, Cho A, et al. Dentin sialoprotein and dentin phosphoprotein have distinct roles in dentin mineralization. Matrix Biol: J Int Soc Matrix Biol 2009;28:221–9.
[44] Goldberg M, Kulkarni AB, Young M, Boskey A. Dentin: structure, composition and mineralization. Front Biosci (Elite Ed) 2011;3:711–35.
[45] George A, Sabsay B, Simonian PA, Veis A. Characterization of a novel dentin matrix acidic phosphoprotein. Implications for induction of biomineralization. J Biol Chem 1993;268:12624–30.
[46] He G, Dahl T, Veis A, George A. Dentin matrix protein 1 initiates hydroxyapatite formation in vitro. Connect Tissue Res 2003;44(Suppl 1):240–5.
[47] He G, George A. Dentin matrix protein 1 immobilized on type I collagen fibrils facilitates apatite deposition in vitro. J Biol Chem 2004;279:11649–56.
[48] Feng JQ, Ward LM, Liu S, Lu Y, Xie Y, Yuan B, et al. Loss of DMP1 causes rickets and osteomalacia and identifies a role for osteocytes in mineral metabolism. Nat Genet 2006;38:1310–5.
[49] Almushayt A, Narayanan K, Zaki AE, George A. Dentin matrix protein 1 induces cytodifferentiation of dental pulp stem cells into odontoblasts. Gene Ther 2006;13:611–20.
[50] Narayanan K, Srinivas R, Ramachandran A, Hao J, Quinn B, George A. Differentiation of embryonic mesenchymal cells to odontoblast-like cells by overexpression of dentin matrix protein 1. Proc Nat Acad Sci USA 2001;98:4516–21.
[51] Chaussain C, Eapen AS, Huet E, Floris C, Ravindran S, Hao J, et al. MMP2-cleavage of DMP1 generates a bioactive peptide promoting differentiation of dental pulp stem/progenitor cell. Eur Cells Mat 2009;18:84–95.
[52] Shi Z, Huang X, Cai Y, Tang R, Yang D. Size effect of hydroxyapatite nanoparticles on proliferation and apoptosis of osteoblast-like cells. Acta Biomater 2009;5:338–45.
[53] Lin S, Van den Bergh W, Baker S, Jones JR. Protein interactions with nanoporous sol–gel derived bioactive glasses. Acta Biomater 2011;7:3606–15.
[54] Webster TJ, Ergun C, Doremus RH, Siegel RW, Bizios R. Specific proteins mediate enhanced osteoblast adhesion on nanophase ceramics. J Biomed Mater Res 2000;51:475–83.
[55] Wittenburg G, Lauer G, Oswald S, Labudde D, Franz CM. Nanoscale topographic changes on sterilized glass surfaces affect cell adhesion and spreading. J Biomed Mater Res, Part A 2013.
[56] Misra SK, Mohn D, Brunner TJ, Stark WJ, Philip SE, Roy I, et al. Comparison of nanoscale and microscale bioactive glass on the properties of P(3HB)/Bioglass composites. Biomaterials 2008;29:1750–61.
[57] Paranjpe A, Smoot T, Zhang H, Johnson JD. Direct contact with mineral trioxide aggregate activates and differentiates human dental pulp cells. J Endod 2011;37:1691–5.
[58] Sarkar NK, Caicedo R, Ritwik P, Moiseyeva R, Kawashima I. Physicochemical basis of the biologic properties of mineral trioxide aggregate. J Endod 2005;31:97–100.
[59] Kiba W, Imazato S, Takahashi Y, Yoshioka S, Ebisu S, Nakano T. Efficacy of polyphasic calcium phosphates as a direct pulp capping material. J Dent 2010;38:828–37.
[60] Gronthos S, Mankani M, Brahim J, Robey PG, Shi S. Postnatal human dental pulp stem cells (DPSCs) in vitro and in vivo. Proc Nat Acad Sci USA 2000;97:13625–30.
[61] Guo HY, Wu BL, Guo XM, Yang C, Xu P, Wang CY. Reconstruction of dentin-pulp complex structure by tissue engineering technology. Zhonghua kou qiang yi xue za zhi [Chinese J Stomatol] 2005;40:511–4.
[62] Alongi DJ, Yamaza T, Song Y, Fouad AF, Romberg EE, Shi S, et al. Stem/progenitor cells from inflamed human dental pulp retain tissue regeneration potential. Reg Med 2010;5:617–31.
[63] Nowicka A, Lipski M, Parafiniuk M, Sporniak-Tutak K, Lichota D, Kosierkiewicz A, et al. Response of human dental pulp capped with biodentine and mineral trioxide aggregate. J Endod 2013;39:743–7.

[64] Parolia A, Kundabala M, Rao NN, Acharya SR, Agrawal P, Mohan M, et al. A comparative histological analysis of human pulp following direct pulp capping with Propolis, mineral trioxide aggregate and Dycal. Aust Dent J 2010;55:59–64.
[65] Tabarsi B, Parirokh M, Eghbal MJ, Haghdoost AA, Torabzadeh H, Asgary S. A comparative study of dental pulp response to several pulpotomy agents. Int Endod J 2010;43:565–71.
[66] Shalumon KT, Sowmya S, Sathish D, Chennazhi KP, Nair SV, Jayakumar R. Effect of incorporation of nanoscale bioactive glass and hydroxyapatite in PCL/chitosan nanofibers for bone and periodontal tissue engineering. J Biomed Nanotechnol 2013;9:430–40.
[67] Valenzuela F, Covarrubias C, Martinez C, Smith P, Diaz-Dosque M, Yazdani-Pedram M. Preparation and bioactive properties of novel bone-repair bionanocomposites based on hydroxyapatite and bioactive glass nanoparticles. J Biomed Mater Res B Appl Biomater 2012;100:1672–82.
[68] Mistry S, Kundu D, Datta S, Basu D. Effects of bioactive glass, hydroxyapatite and bioactive glass – hydroxyapatite composite graft particles in the treatment of infrabony defects. J Indian Soc Periodontol 2012;16:241–6.
[69] Carlisle EM. Silicon: a requirement in bone formation independent of vitamin D1. Calcif Tissue Int 1981;33:27–34.
[70] Carlisle EM. Silicon: a possible factor in bone calcification. Science 1970;167:279–80.
[71] Varanasi VG, Leong KK, Dominia LM, Jue SM, Loomer PM, Marshall GW. Si and Ca individually and combinatorially target enhanced MC3T3-E1 subclone 4 early osteogenic marker expression. J Oral Implantol 2012;38:325–36.
[72] Honda M, Kikushima K, Kawanobe Y, Konishi T, Mizumoto M, Aizawa M. Enhanced early osteogenic differentiation by silicon-substituted hydroxyapatite ceramics fabricated via ultrasonic spray pyrolysis route. J Mater Sci - Mater Med 2012;23:2923–32.
[73] Reffitt DM, Ogston N, Jugdaohsingh R, Cheung HF, Evans BA, Thompson RP, et al. Orthosilicic acid stimulates collagen type 1 synthesis and osteoblastic differentiation in human osteoblast-like cells in vitro. Bone 2003;32:127–35.
[74] Oguntebi B, Clark A, Wilson J. Pulp capping with Bioglass and autologous demineralized dentin in miniature swine. J Dent Res 1993;72:484–9.
[75] Oguntebi BR, Heaven T, Clark AE, Pink FE. Quantitative assessment of dentin bridge formation following pulp-capping in miniature swine. J Endod 1995;21:79–82.
[76] Sepulveda P, Jones JR, Hench LL. Characterization of melt-derived 45S5 and sol–gel-derived 58S bioactive glasses. J Biomed Mater Res 2001;58:734–40.